Cerebral Cortex September 2010;20:2055–2068
doi:10.1093/cercor/bhp280
Advance Access publication December 23, 2009

# Life-Span Changes of the Human Brain White Matter: Diffusion Tensor Imaging (DTI) and Volumetry

Lars T. Westlye[1], Kristine B. Walhovd[1], Anders M. Dale[2,3,4], Atle Bjørnerud[5,6,7], Paulina Due-Tønnessen[6], Andreas Engvig[1], Håkon Grydeland[1], Christian K. Tamnes[1], Ylva Østby[1] and Anders M. Fjell[1]

[1]Department of Psychology, Center for the Study of Human Cognition, University of Oslo, Blindern, 0317 Oslo, Norway, [2]Multimodal Imaging Laboratory, University of California, La Jolla, CA 92093, USA, [3]Department of Radiology, University of California, San Diego, CA 92103, USA, [4]Department of Neurosciences, University of California, San Diego, CA 92103, USA, [5]Department of Medical Physics, Rikshospitalet University Hospital, 0027 Oslo, Norway, [6]Department of Physics, University of Oslo, Blindern, 0316 Oslo, Norway and [7]Department of Radiology, Rikshospitalet University Hospital, 0027 Oslo, Norway

**Magnetic resonance imaging volumetry studies report inverted U-patterns with increasing white-matter (WM) volume into middle age suggesting protracted WM maturation compared with the cortical gray matter. Diffusion tensor imaging (DTI) is sensitive to degree and direction of water permeability in biological tissues, providing in vivo indices of WM microstructure. The aim of this cross-sectional study was to delineate age trajectories of WM volume and DTI indices in 430 healthy subjects ranging 8–85 years of age. We used automated regional brain volume segmentation and tract-based statistics of fractional anisotropy, mean, and radial diffusivity as markers of WM integrity. Nonparametric regressions were used to fit the age trajectories and to estimate the timing of maximum development and deterioration in aging. Although the volumetric data supported protracted growth into the sixth decade, DTI indices plateaued early in the fourth decade across all tested regions and then declined slowly into late adulthood followed by an accelerating decrease in senescence. Tractwise and voxel-based analyses yielded regional differences in development and aging but did not provide ample evidence in support of a simple last-in-first-out hypothesis of life-span changes.**

**Keywords:** aging, development, DTI, FA, MRI, white-matter microstructure

## Introduction

Cerebral white matter (WM) consists largely of densely packed myelinated neuronal axons, and efficient cognitive processing relies on the integrity of these pathways (Olesen et al. 2003; Tuch et al. 2005; Liston et al. 2006; Fields 2008; Kennedy and Raz 2009a; Perry et al. 2009; Westlye, Walhovd, Bjørnerud, et al. 2009; Zahr et al. 2009). An association between WM changes and cognitive decline in aging (O'Sullivan et al. 2001; Davis et al. 2009; Kennedy and Raz 2009a) and degenerative diseases (Head et al. 2004; Salat et al. forthcoming) has been established, conjunctively referred to as the disconnection hypothesis (Bartzokis 2004). In vitro studies report marked alterations in myelinated fibers in aged humans (Tang et al. 1997; Marner et al. 2003) and primates (Peters 2002a, 2002b; Sandell and Peters 2003). Human magnetic resonance imaging (MRI) volumetry suggests an inverted U pattern with protracted growth extending into the fifth or sixth decade with subsequent accelerating decrease (Courchesne et al. 2000; Jernigan et al. 2001; Resnick et al. 2003; Allen et al. 2005; Fotenos et al. 2005; Raz et al. 2005; Ikram et al. 2008; Salat, Greve, et al. 2009; Walhovd et al. forthcoming). Possible neurobiological explanations for these changes are numerous, including axonal (re)wiring and myelination in development (Lebel et al. 2008; Tamnes et al. forthcoming), loss and shrinkage of myelinated fibers (Tang et al. 1997; Peters 2002a; Marner et al. 2003), and accumulation of redundant myelin in aging (Wozniak and Lim 2006).

Diffusion tensor imaging (DTI) is sensitive to degree and direction of water molecule permeability (Beaulieu 2002; Le Bihan 2003), enabling in vivo imaging of WM microstructure, yielding complementary information to volumetry (Abe et al. 2008; Fjell et al. 2008). A commonly reported diffusivity measure is fractional anisotropy (FA), indexing directional coherence of water displacement (Pierpaoli and Basser 1996). Age-related decreases in FA is well documented (O'Sullivan et al. 2001; Head et al. 2004; Pfefferbaum et al. 2005; Salat, Tuch, Greve, et al. 2005; Charlton et al. 2006; Sullivan and Pfefferbaum 2006; Ardekani et al. 2007; Grieve et al. 2007; Abe et al. 2008; Hugenschmidt et al. 2008; Davis et al. 2009; Kennedy and Raz 2009a). However, large-scale analyses showing nonlinear life-span trajectories are lacking.

Demonstrations of a nonlinear pattern of WM volume changes have nurtured the hypothesis of protracted WM maturation into middle age (Bartzokis 2004), but it is not known whether this pattern holds for WM diffusivity as well. Because evidence indicates that WM development is a slow process that starts in infancy and continues for decades (Giedd et al. 1999; Klingberg et al. 1999; Paus et al. 1999; Bartzokis et al. 2001; Ashtari et al. 2007; Lenroot et al. 2007; Giorgio et al. 2008; Lebel et al. 2008; Paus et al. 2008; Giorgio et al. 2010; Østby et al. 2009; Tamnes et al. forthcoming), an accurate description of age-related changes should be based on large continuous samples including children, adults, and the elderly (Raz et al. 2005). We are aware of only 1 full-brain life-span DTI study. Hasan et al. (2007) reported quadratic curves of whole-brain WM FA and mean diffusivity (MD) in a sample spanning 7–67 years of age but did not explore possible regional variability. Thus, little is known about regional DTI trajectories across the life span. As previously reported, WM volume tends to show a 3-phasic life-span development with accelerating changes in the earliest and latest phases of life and a relatively stable plateau in early and middle adulthood (Courchesne et al. 2000; Jernigan et al. 2001; Raz et al. 2004, 2005). However, it is not known to what degree life-span diffusivity changes support the suggested protracted WM development inferred from volumetric studies.

The aim of the present study was to explore the notion of protracted WM maturation by delineating regional life-span

trajectories of diffusivity and WM volume in 430 healthy subjects aged 8–85 years using automated whole-brain volume segmentation and tract-based statistics of DTI indices of WM integrity. DTI indices were sampled globally, voxelwise, and per fasciculus covering large association tracts important for a wide array of cognitive functions. The sampled fiber tracts included the anterior thalamic radiation (ATR), dorsal cingulum bundle (CG), the parahippocampal cingulum bundle (CH), the corticospinal tract (CST), the inferior longitudinal fasciculus (ILF), the superior longitudinal fasciculus (SLF), the uncinate fasciculus (UF), the forceps minor (Fmin), and the forceps major (Fmaj). Voxelwise effects were tested using tract-based spatial statistics (TBSS) implemented in FSL (http://www.fmrib.ox.ac.uk/fsl/). Global and lobar WM volumes were computed using an automatic gyral WM segmentation scheme in FreeSurfer (http://surfer.nmr.mgh.harvard.edu/).

Based on autopsy studies of myelination in human infants, one would expect a sequence of development with the earliest maturation seen around the central sulcus, including the CST, and then a posterior–anterior gradient with earlier maturation in posterior compared with anterior areas (Yakovlev and Lecours 1967; Kinney et al. 1988). To the degree that DTI indices reflect myelin-related processes, the same general tendencies may be expected in the current sample. In line with previous developmental DTI studies (Lebel et al. 2008; Tamnes et al. forthcoming), we expected a relatively protracted maturation in frontotemporal connections compared with other regions. Further, suggested by evidence of an inversed ontogenetic WM deterioration in aging (Courchesne et al. 2000; Raz 2000; Bartzokis 2004; Kochunov et al. 2007; Davis et al. 2009; Raz and Kennedy 2009; Kennedy and Raz 2009b), so-called retrogenesis, we expected early age-related changes in areas showing protracted maturation. We also expected elevated vulnerability to age-related decreases in frontal WM (Head et al. 2004; Salat, Tuch, et al. 2005). Thus, we hypothesized that the CG, CH, the UF, and the Fmin would be among the latest to fully mature and earliest to show age-related deterioration. In contrast, we expected relatively early maturation and late age-related deterioration in areas encompassing the CST.

## Materials and Methods

### *Sample*

The sample was drawn from the first wave of 2 longitudinal research projects at the Center for the Study of Human Cognition at the University of Oslo: "Neurocognitive Development" (Østby et al. 2009; Tamnes et al. forthcoming) and "Cognition and Plasticity through the Life-Span" (Fjell et al. 2008; Westlye, Walhovd, Bjørnerud, et al. 2009). The study was approved by the Regional Ethical Committee of Southern Norway (REK-Sør). The participants were recruited through newspaper advertisements and selected from among students and employees of the University of Oslo. Further details regarding recruitment and enrolment are given elsewhere (Fjell et al. 2008; Østby et al. 2009; Westlye, Walhovd, Bjørnerud, et al. 2009; Tamnes et al. forthcoming). We obtained written informed consent from all participants ⩾12 years and from parents for participants <18 years of age. Oral informed consent was given by participants <12 years of age. Four hundred and thirty healthy participants (54.9% females) aged 8–85 years (mean: 41.6, standard deviation [SD]: 21.9) were included. Demographic details per decade and in the total sample are summarized in Table 1. The participants were not evenly distributed across the life span with a higher number of participants in transitional phases where we expected large changes to take place (childhood to young adulthood, as well as middle adulthood where age-related changes could start accelerating). This uneven distribution of participants can potentially influence conventional least-square regressions, but is less likely to affect nonparametric local regressions used for the main analyses in the present study (see Statistical analyses).

There was no correlation between sex and age (Pearson's $r = -0.02$, $P > 0.68$, with females coded as 0 and males as 1). All subjects were right handed native Norwegian speakers. The participants were not subjected to a full medical assessment but were screened using a standardized health interview prior to inclusion in the study. Participants with a history of self- or parent-reported neurological or psychiatric conditions including clinically significant stroke, serious head injury, untreated hypertension, diabetes, and use of psychoactive drugs within the last 2 years were excluded. Further, participants reporting worries concerning their cognitive status, including memory function, were excluded. All subjects above 20 years of age scored <16 on Beck Depression Inventory (Beck and Steer 1987) and subjects above 40 years of age ⩾26 on Mini Mental State Examination (Folstein et al. 1975; Bravo and Hebert 1997). General cognitive abilities were assessed by Wechsler Abbreviated Scale of Intelligence (WASI) (Wechsler 1999). All subjects scored within normal IQ range (82–145).

All subjects' MR scans were examined by a neuroradiologist and deemed free of significant anomalies. Four hundred and thirty-seven subjects were enrolled in the study after the initial health screening. Four subjects were excluded due to missing DTI data or motion artifacts, 1 was excluded due to age (>90 years, which created a gap of missing data points on the continuous age scale) and 2 were excluded after radiological evaluation, yielding a final sample of 430 subjects.

### *MRI Acquisition*

Imaging was performed using a 12-channel head coil on a 1.5-T Siemens Avanto scanner (Siemens Medical Solutions, Erlangen, Germany) at Rikshospitalet University Hospital, Oslo. For diffusion weighted imaging

**Table 1**
Sample descriptives by age group and total

| Age group (years) | *n* | Females *n* (%) | FIQ[a] mean (SD) | MMS[b] mean (SD) | Years education[c] mean (SD) | Age mean years (SD) |
|---|---|---|---|---|---|---|
| 8.0–10.00 | 20 | 9 (45) | 105.0 (11.6) | n.a. | n.a. | 9.0 (0.5) |
| 10.01–20.00 | 89 | 46 (52) | 109.9 (10.6) | n.a. | n.a. | 15.1 (2.9) |
| 20.01–30.00 | 54 | 28 (52) | 112.4 (7.1) | n.a. | 15.1 (1.9) | 24.0 (2.6) |
| 30.01–40.00 | 40 | 25 (63) | 115.1 (8.4) | n.a. | 17.0 (2.6) | 35.1 (3.1) |
| 40.01–50.00 | 43 | 27 (63) | 114.8 (7.2) | 29.3 (0.7) | 15.2 (2.2) | 46.2 (3.1) |
| 50.01–60.00 | 74 | 44 (59) | 112.9 (7.9) | 29.2 (0.8) | 15.3 (2.1) | 54.9 (2.7) |
| 60.01–70.00 | 75 | 39 (52) | 117.7 (10.7) | 29.1 (0.9) | 16.3 (3.2) | 65.4 (3.1) |
| 70.01–80.00 | 25 | 13 (52) | 115.4 (9.4) | 28.7 (1.2) | 14.5 (3.4) | 74.8 (2.7) |
| 80.01–85.00 | 10 | 5 (50) | 119.2 (16.4) | 28.6 (0.8) | 14.5 (2.7) | 82.6 (1.4) |
| Total | 430 | 236 (55) | 113.4 (9.9) | 29.0 (2.0) | 15.6 (2.6) | 41.6 (21.9) |

[a]Full-scale IQ (FIQ) was estimated from the WASI (Wechsler 1999) subtests matrices, block design, vocabulary, and similarities. For 39 subjects, only matrices and vocabulary was available. WASI scores were available for 429 subjects.
[b]MMS (Folstein et al. 1975) scores not available for subjects below 40 years of age
[c]Years of education was not estimated for subjects below 20 years. Most subjects between 20 and 30 years of age were recruited among university students, and years of education were calculated as number of years completed at time of assessment.

a single-shot twice-refocused spin-echo echo planar imaging pulse sequence with 30 diffusion sensitized gradient directions and the following parameters was used: repetition time (TR)/echo time (TE) = 8200 ms/82 ms, *b*-value = 700 s/mm$^2$, voxel size = 2.0 × 2.0 × 2.0 mm, and 64 axial slices. The sequence was repeated in 2 successive runs with 10 $b$ = 0 and 30 diffusion weighted images collected per run. Acquisition time was 11 min 21 s. This sequence is optimized to minimize eddy current–induced distortions (Reese et al. 2003). The 2 acquisitions were averaged during postprocessing to increase signal-to-noise ratio (SNR).

The pulse sequence used for volumetric analyses were 2 repeated T1-weighted magnetization prepared rapid gradient echo (MP-RAGE), with the following parameters: TR/TE/time to inversion (TI)/FA = 2400 ms/3.61 ms/1000 ms/8°, matrix 192 × 192, field of view = 240, voxel size = 1.25 × 1.25 × 1.20 mm, and 160 sagittal slices. Scanning time was 7 min 42 s. The 2 runs were averaged during postprocessing to increase SNR. Due to motion artifacts, only 1 scan was available for 25 of the participants below 19 years of age.

The protocol also included a 176 slices sagittal 3D T2-weighted turbo spin-echo sequence (TR/TE = 3390/388 ms), and a 25 slices coronal FLAIR sequence (TR/TE = 7000–9000/109 ms) used for clinical assessment.

All data sets were processed and analyzed at the Neuroimaging Analysis Lab, Center for the Study of Human Cognition, University of Oslo, with additional use of computing resources from the Titan High Performance Computing facilities (http://hpc.uio.no/index.php/Titan) at the University of Oslo.

### *DTI Analysis*

Image analyses and tensor calculations were done using FSL (Smith et al. 2004; Woolrich et al. 2009). Initially, each DTI volume was affine registered to the T2-weighted $b$ = 0 volume using FLIRT (Jenkinson and Smith 2001). This corrected for motion between scans and residual eddy-current distortions present in the diffusion weighted images. After averaging of the 2 acquisitions and removal of nonbrain tissue (Smith 2002) FA, eigenvector and -value maps were computed. We defined MD as the mean of all 3 eigenvalues $[(\lambda_1 + \lambda_2 + \lambda_3)/3]$ and radial diffusivity (RD) as the mean of the second and third eigenvalue $[(\lambda_2 + \lambda_3)/2]$. Note that the nomenclature ("mean" and "radial" diffusivity) pertains to the eigenvalues of the diffusion tensor and not necessarily to the underlying brain tissue (Wheeler-Kingshott and Cercignani 2009).

Next, all individuals' FA volumes were skeletonized and transformed into a common space as employed in TBSS (Smith et al. 2006, 2007). Briefly, all volumes were nonlinearly warped to the FMRIB58_FA template, which is supplied with FSL, by use of local deformation procedures performed by FNIRT (Andersson et al. 2007a, 2007b), a nonlinear registration toolkit using a $b$-spline representation of the registration warp field (Rueckert et al. 1999).

The common template used in the present study is a high-resolution average of 58 FA volumes from healthy male and female subjects aged 20–50 years. It is expected that amount of warping needed to align each individual FA volume to this template would commensurate with the distance in each participant's age from the age of the subjects used to build the template. All warped FA volumes were visually inspected for accuracy, which is especially pertinent when analyzing life-span data sets with relatively large individual variability in brain size and architecture. A critical validation of the procedure can be obtained by inspecting the resulting warped volumes. We computed the mean warped FA volumes for each decade to enable visual inspection of the registration between age groups. Note that all participants >70 years of age were pooled. Figure 1 (left panels) shows the resulting mean warped images for each group. In our experience, FNIRT performed the native-to-standard warping adequately across age groups. For comparison and validation of the nonlinear registration, Figure 1 (right panels) depicts the mean affine registered FA volumes. The affine registration to the common template was done using FLIRT (Jenkinson and Smith 2001).

Next, a mean FA volume of all subjects was generated and thinned to create a mean FA skeleton representing the centers of all common tracts. We thresholded and binarized the mean skeleton at FA > 0.25 to reduce the likelihood of partial voluming in the borders between tissue

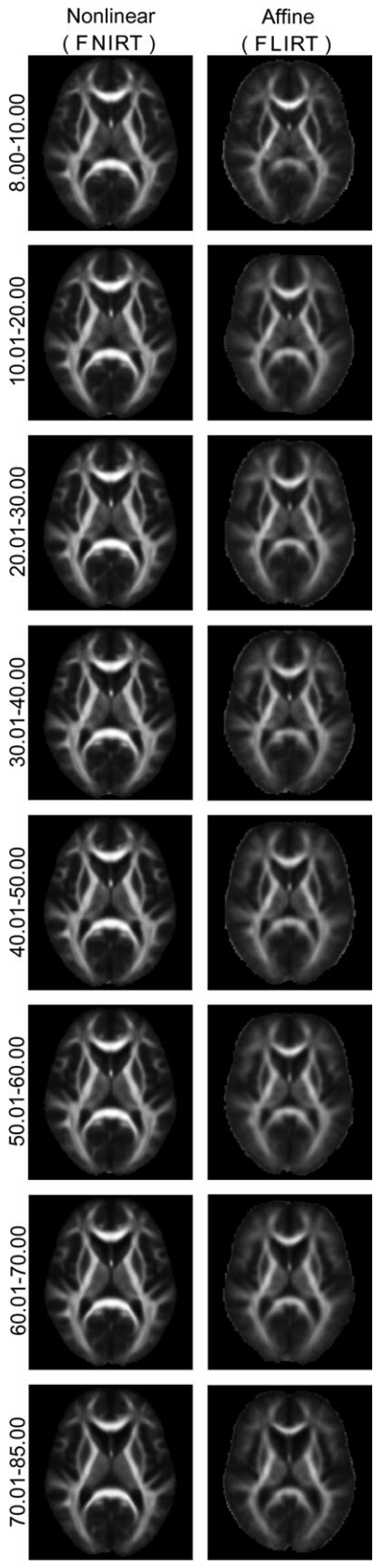


**Figure 1.** Nonlinear warping to a common template in different age groups. The figure shows the mean nonlinearly warped (left) and the mean affine registered (right) FA volumes for each decade. The volumes were aligned to the FMRIB58_FA template (www.fmrib.ox.ac.uk/fsl/data/FMRIB58_FA.html). Participants > 70 years of age were pooled.

classes, yielding a mask of 107,193 WM voxels. Individual FA values were warped onto this mean skeleton mask by searching perpendicular from the skeleton for maximum FA values. Using maximum FA from the centers of the tracts further minimizes confounding effects due to partial voluming (Smith et al. 2006). The resulting tract invariant skeletons for each participant were fed into voxelwise permutation based cross-subject statistics. Similar warping and analyses were employed on MD and RD data, yielding MD and RD skeletons sampled from voxels with FA > 0.25. Further, binary masks based on the probabilistic JHU white-matter tractography atlas (Wakana et al. 2004; Mori et al. 2005; Hua et al. 2008) were created with a probability threshold of 5%, chosen to accommodate individual variation in WM architecture (Westlye, Walhovd, Bjørnerud, et al. 2009).

We chose 7 major WM tracts in each hemisphere (ATR, CG, CH, ILF, SLF, UF, and CST) and 2 commissural tracts (Fmin and Fmaj) as tracts of interest (TOIs). Voxels intersecting both the skeleton and the TOI were used to delineate life-span trajectories of WM microstructure. The bilateral tracts were averaged for main analyses, but per hemisphere trajectories are available online (Supplementary Figs. 1 and 2).

### *Volumetric Analyses*

We estimated regional WM volumes using FreeSurfer 4.1 by means of an automated surface reconstruction scheme described in detail elsewhere (Dale et al. 1999; Fischl, Sereno, and Dale 1999; Fischl, Sereno, Tootell, and Dale 1999; Fischl and Dale 2000; Fischl et al. 2001; Segonne et al. 2004). Briefly, a representation of the gray matter (GM)/WM boundary was reconstructed (Dale et al. 1999) using intensity and continuity information from the entire MR volume in segmentation and deformation procedures. The cortical surface was automatically parcellated based on 1) the probability of each label at each location in a surface-based atlas space, based on a manually parcellated training set; 2) local curvature information; and 3) contextual information, encoding spatial neighborhood relationships between labels resulting in 33 surface-based regions (Fischl et al. 2004; Desikan et al. 2006).

WM voxels within a distance of 5 mm from the cortical surface was labeled according to the label of the nearest cortical vertex (Fjell et al. 2008; Salat, Greve, et al. 2009) yielding 33 bilateral gyral WM segmentations, each corresponding to a cortical area. The WM voxels not assigned to a surface area were labeled deep WM. All surface labels were manually inspected for accuracy. Areas segmented by FreeSurfer as hypointense WM areas ("dark spots") based on the MP-RAGES were not included in the WM volumes. We combined parcels into larger subsets of bilateral lobe based regions (frontal, parietal, temporal, and occipital lobe) in addition to the cingulate gyrus, corpus callosum, and deep and total WM volume. The corpus callosum was automatically defined in the probabilistic volume-based segmentation scheme in FreeSurfer. The subsets and composite WM parcels are shown in Supplementary Table 1. The reliability of the gyral volumetric segmentation procedure has been established across 2 scan sessions in young healthy individuals and was also found sensitive to the effects of normal aging and Alzheimer's disease (AD) (Salat, Greve, et al. 2009). We used intracranial volume (ICV) to adjust the volumetric data for cranial vault size. ICV was estimated by an atlas-based normalization procedure, where the atlas scaling factor is used as a proxy for ICV, shown to correlate 0.93 with manually derived ICV (Buckner et al. 2004).

The surface reconstruction and segmentation procedures are run automatically but require supervision of the accuracy of the spatial registration and tissue segmentations. The types of errors that most often prompted user intervention in the current data sets were insufficient removal of nonbrain tissue (typically dura/vessels adjacent to the cortex, especially in the orbitofrontal cortices). In addition, in presence of local artifacts, small parts of WM may mistakenly be segmented as GM, thus obscuring the WM/GM boundary. All volumes were visually checked for accuracy, and segmentation errors were manually corrected by trained operators. Minor manual edits were performed on most subjects (>80%), usually restricted to removal of nonbrain tissue orbitofrontally included within the cortical boundary.

### *Statistical Analyses*

Voxel-based DTI analyses were performed using permutation-based inference (Nichols and Holmes 2002) as implemented in "randomise," part of FSL. We tested for linear and quadratic effects of age on FA, MD, and RD with general linear models (GLMs) while regressing out the effects of sex. Threshold-free cluster enhancement (Smith and Nichols 2009) was used in order to avoid the arbitrariness involved in setting smoothing levels and thresholds for cluster size inference. Five thousand permutations were performed for each contrast. Statistical $P$ value maps were thresholded at $P < 0.05$ corrected for multiple comparisons across space.

Curve fitting on ROIs and TOIs was performed using functions freely available through the statistical environment $R$ (http://www.r-project.org/). First, we fitted data by ordinary least-square (OLSs) regressions. Due to the age span of the included participants, we expected strong nonmonotonic effects of age. Thus, only parameters from the quadratic regressions are presented. These are the unique effects of age$^2$ after regressing out the linear effects of age and sex. The OLS regressions were performed to enable comparisons with previous studies and to establish nonlinear relationships with age. Secondly, fitting was made by locally weighted polynomial regression (LOESS) (Cleveland and Devlin 1988) in order to delineate age-related WM changes without enforcing a common parametric function on the full data set as is the case with OLS regressions. Because we used LOESS to describe age trajectories and not to test hypotheses of certain predefined trajectories (e.g., linear vs. quadratic), OLS regressions were first used to test whether the null hypothesis of linear relationships could be rejected. Briefly, a polynomial fit is made iteratively on a subset of the data in a moving fashion. For the fit at age $X$, the fit is made using values in a neighborhood of $X$, each weighted by the distance from $X$. The size of the neighborhood is defined by alpha, and for alpha < 1, the neighborhood includes a proportion alpha of the values. Data were fitted in 4 iterations with alpha = 0.75. Observed and fitted values of FA, MD, RD, and standardized residuals of WM volumes after regressing out ICV were plotted as a function of age to display age-related variability and predicted trajectories. Sex was regressed out in all analyses. Although the global analyses were performed on all estimated measures, the regional analyses were repeated for WM volume, FA, and RD only.

To explore the spatial variability in maturation and aging, we performed robust LOESS (rLOESS) fitting on each voxel in the skeletonized FA volume using custom Matlab routines. Age at maximum FA was estimated for every voxel and mapped back to the skeleton. Also, age when FA was equal to 50% of the distance between maximum FA and FA at maximum age was estimated and mapped back to the skeleton. Thus, every skeleton voxel was represented with a value of age at maturational peak and age at 50% of total estimated age-related reduction. For these analyses, the warped FA volumes were spatially smoothed with a 3D Gaussian kernel with sigma = 2 mm (which approximates a full width at half maximum of 4.7 mm) prior to the skeletonization and smoothing procedure. Only voxels showing significant inverse life-span U-patterns in the TBSS analyses were included in the voxel-based rLOESS analyses.

## Results

### *Global Analyses*

#### *FA*

Figure 2 (upper rows) shows the results from GLMs testing linear and quadratic effects of age on FA across the skeleton. Red color denotes significant voxels thresholded at $P < 0.05$ corrected for multiple comparisons across space. As expected, FA was significantly related to age in large portions of the brain. Of the skeleton voxels, 83.8% showed a unique significant negative linear relationship with age and 65.6% of the voxels showed a unique significant inverse U-shaped relationship with age. Mean FA from the whole skeleton is plotted as a function of age in the upper right corner of Figure 2. As evident from the plot, and as predicted from the TBSS analyses, strong quadratic effects of age are seen. Estimated age at maximum FA was 29.1

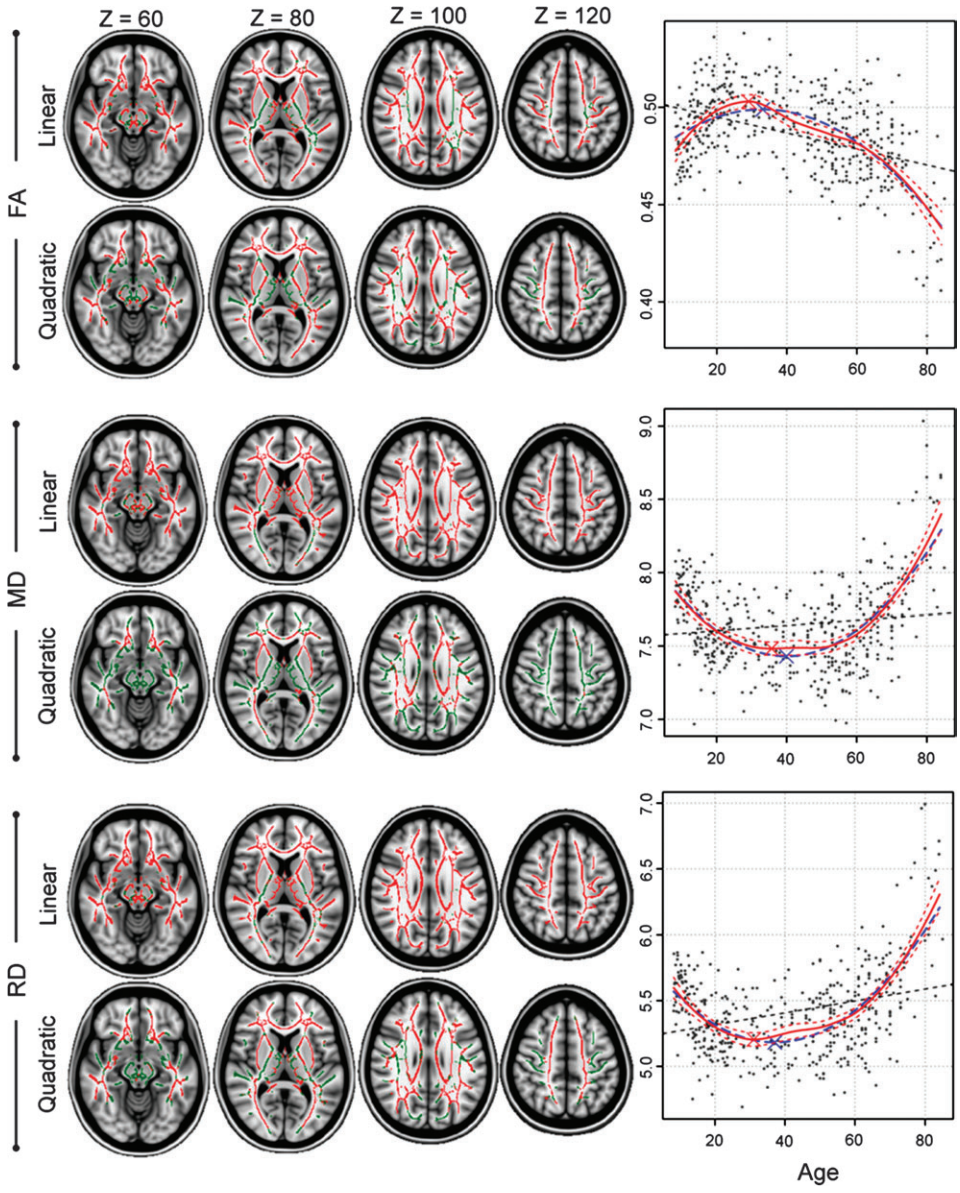


**Figure 2.** GLMs and global fitting of DTI indices across the life span. Head models: Results from GLMs testing linear and quadratic fits for FA (upper rows), mean MD ($10^{-4} \times mm^2/s$) (middle rows) and RD ($10^{-4} \times mm^2/s$) in the TBSS skeleton superimposed on transverse slices of a template brain. The numbers denote the Montreal Neurological Institute *Z*-voxel coordinates. Red areas indicate voxels with significant ($P < 0.05$, corrected for multiple comparisons across space) effect of age (linear) or age$^2$ (quadratic) on the different measures. Green areas are the nonsignificant remains of the skeleton. Scatter plots: Individual mean skeleton FA (upper), MD (middle), and RD (bottom) plotted as a function of age. Black dotted lines denote the linear, blue lines the quadratic and the red solid lines the LOESS fits. The red dotted lines represent the 95% confidence band of the LOESS fit. Blue and red crosses mark the estimated maxima (FA) and minima (MD/RD) for the quadratic and LOESS fits, respectively.

years. Table 2 summarizes the results from the parametric fit as well as age at the LOESS estimated maxima/minima for FA, MD, and RD.

*MD*

Figure 2 (middle rows) shows the results from the global MD analyses. Large areas of significant positive linear and U-shaped relationships with age were found. Of the skeleton voxels, 92.8% showed a unique significant positive linear relationship and 45.6% of the voxels showed a unique significant U-shaped relationship with age. As outlined in Table 2, age at the LOESS estimated minimum MD was 35.7 years.

*RD*

Figure 2 (bottom rows) shows the results from the global RD analyses. Voxel-based GLMs yielded large areas of significant positive linear and quadratic relationships with age. 93.1% of the skeleton voxels showed a unique significant positive linear relationship with age and 53.9% showed a unique significant U-shaped relationship with age. As depicted in Figure 1 and evident in Table 2, age at the LOESS estimated minimum RD was 31.1 years.

*WM Volume*

Table 2 shows the results from least-square regressions with standardized residuals of the total ICV-regressed WM volume as

**Table 2**

Results from OLS regressions with global MRI measures as dependent and sex, age, and age$^2$ as independent variables

| | *t* | *F* | $R^2$ | sig | Age at maxima/minima (years) |
|---|---|---|---|---|---|
| FA | −10.5 | 108.5 | 0.33 | *** | 29.1 |
| MD | 15.2 | 121.8 | 0.36 | *** | 35.7 |
| RD | 14.6 | 138.4 | 0.39 | *** | 31.1 |
| WM volume | −15.1 | 119.3 | 0.36 | *** | 50.1 |

Note: Mean values across the TBSS skeleton were used for FA, D and RD. Standardized residuals after regressing out ICV were used for the volume analysis. $t = t$ value, $F = F$ value, $R^2$ = adjusted $R^2$, Age at maxima/minima = age at LOESS estimated maximum maturation for the different measures.

***$P < 0.0001$.

dependent and sex, age, and age$^2$ as independent variables. Figure 3 (right bottom corner) shows the standardized residuals of total WM volume plotted against age. A significant quadratic fit was found, with LOESS estimated maximum value at 50.1 years.

### *Regional Analyses*

#### *Correlations between Tracts*

Figure 4 shows pseudocolor maps of the correlation matrices for the different fiber tracts for FA (left), MD (middle), and RD (right). The matrices have been arranged so that highly correlated tracts are organized along the diagonal. Except for the 2 cingulum bundles, the correlations between tracts were generally strong. All tracts showed strong correlations between hemispheres.

#### *FA*

Age × FA plots for the TOIs are shown in Figure 5 and results from least-square regressions with age at estimated maxima are outlined in Table 3. All TOIs showed highly significant ($P < 0.001$, Bonferroni corrected) inverted U-shaped relationships with age. Estimated age at maximum FA ranged from 24.0 years in Fmin to 31.8 years in parahippocampal cingulum. As evident from Figure 5, the parahippocampal cingulum bundle revealed a high degree of between subject variability. Median LOESS estimated peak of all TOIs was 28.6 years (SD = 2.6). Supplementary Figure 1 displays age × FA plots per hemisphere.

#### *Regional Variability in Timing of Maturation and Age-Related Deterioration*

Time-lapse renderings illustrating the results from the voxel-based rLOESS analyses are available online. Supplementary Movie 1 shows the anatomical variability of WM maturation as indexed by age at maximum FA value. Supplementary Movie 2 shows the regional variability in age when FA fell below 50% of the difference between maximum FA (peak) and FA at maximum age.

Figure 6 (panel *A*) shows snapshots from Supplementary Movie 1 and cumulative portions of voxels per tract reaching maximum FA as a function of age (panel *B*). Relatively early maturation (<21 years) was seen not only in occipital but also in several frontal areas, including parts of Fmin. All tracts showed similar general patterns, but the portion of matured voxels at the earliest sampled age (8 years) varied between

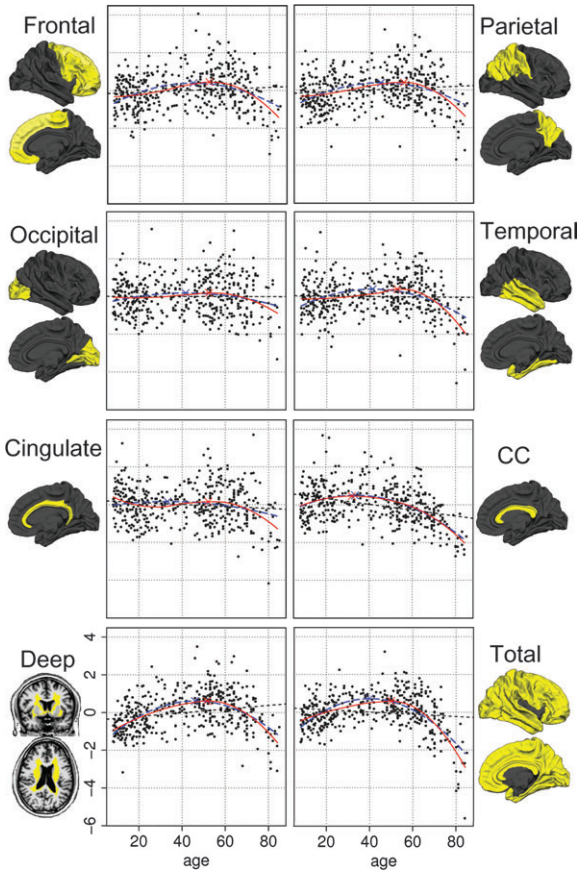


**Figure 3.** WM volumes through the life span. Individual regional and total WM volumes (standardized residuals after regressing out sex and ICV) plotted as a function of age. Black dotted lines denote the linear, blue lines the quadratic and red lines the LOESS fits. Blue and red crosses mark the estimated maxima for the quadratic and LOESS fits, respectively. CC: corpus callosum. Yellow areas denote the surface areas used to estimate the gyral WM volumes.

tracts. For instance, approximately 24% of the CST voxels did not show any further FA increases beyond 8 years of age, whereas this was true for only approximately 2% of the voxels in the dorsal and parahippocampal cingulum bundles. Further, for Fmaj and CST, 50% of the voxels peaked around 20 years of age, whereas the parahippocampal (~27 years) and the dorsal cingulum bundles (~30 years) showed a slower maturation.

Figure 6 (Panels *C* and *D*) shows the timing of estimated age-related WM deterioration. Parts of SLF and CST reached the threshold already at around 30 years of age, followed by areas encompassing parts of the Fmin in the late 40s and posterior areas including the occipital lobes in the early 60s. For most tracts, the vast majority of voxels reached the threshold in the 60s. Relatively early deterioration was seen in CST, where approximately 25% of the voxels had reached the threshold at 55 years of age. For the dorsal cingulum bundle, Fmaj, UF, and Fmin, 25% of the voxels had reached the threshold at 65 years.

#### *RD*

Age × RD plots for each TOI are given in Figure 7 and statistics from the least-square regressions and age at estimated maximum development are outlined in Table 4. All TOIs showed significant ($P < 0.001$, Bonferroni corrected) positive quadratic

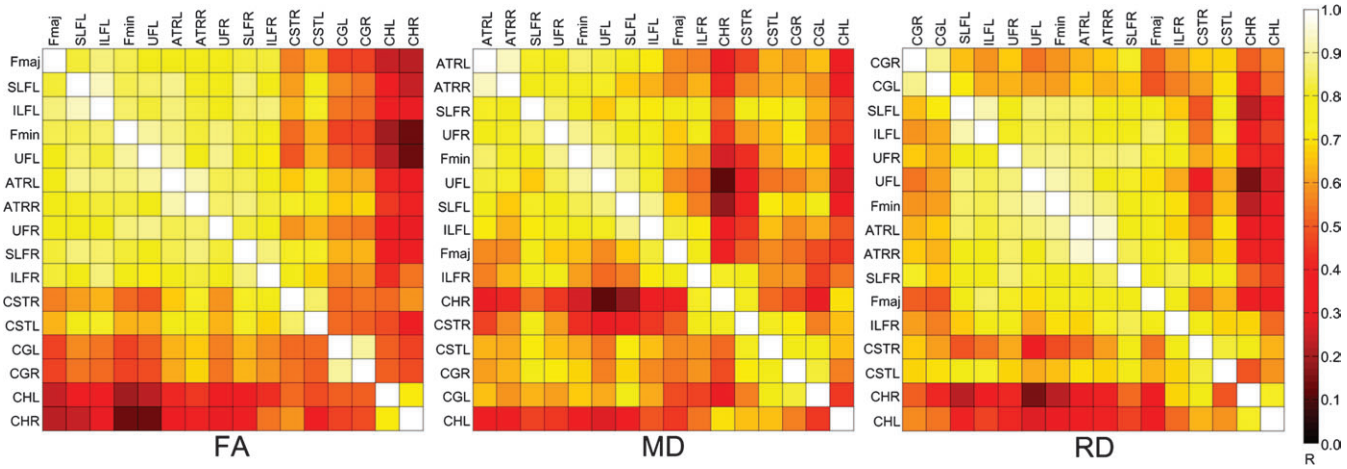


**Figure 4.** Correlations between fiber tracts. The figure shows pseudocolor maps of the correlation matrices for the different fiber tracts for FA (left), MD (middle) and RD (right). The matrices have been arranged so that highly correlated variables are organized along the diagonal. Red/dark colors denote weak and yellow/bright colors denote strong correlations (see color bar on the right).

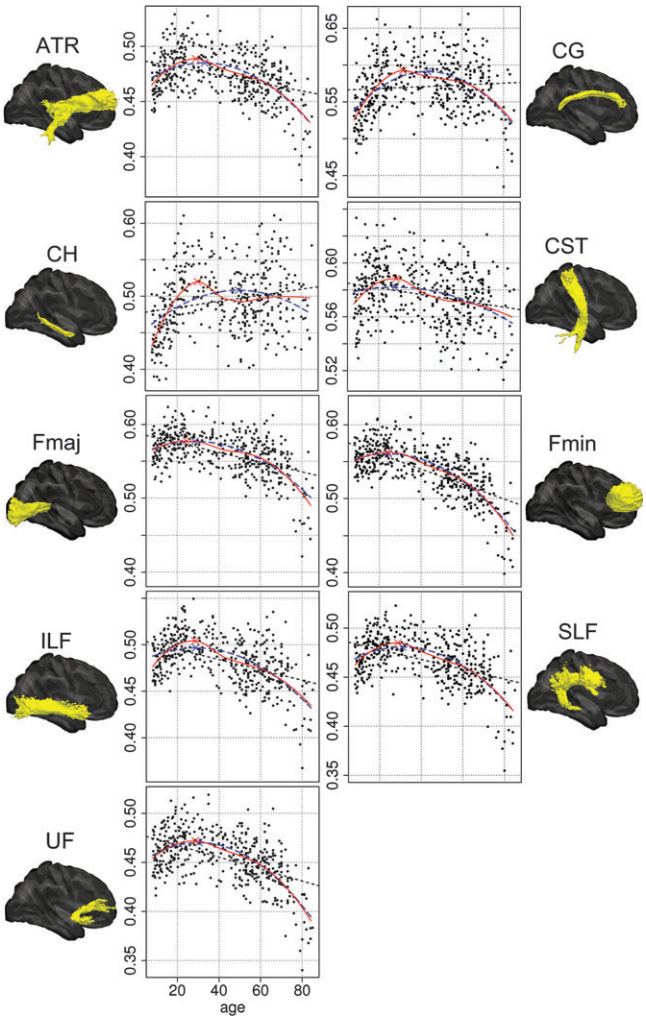


**Figure 5.** Regional FA through the life span. Individual mean FA from the various atlas tract × skeleton intersections plotted as a function of age. Black dotted lines denote the linear, blue lines the quadratic and red lines the LOESS fits. Blue and red crosses mark the estimated maxima for the quadratic and LOESS fits, respectively. The yellow areas represent the probabilistically defined WM tracts used.

**Table 3**
Results from OLS regressions with regional FA values as dependent and sex, age, and age$^2$ as independent variables

| FA | *t* | *F* | $R^2$ | sig | Age at maxima (years) |
|---|---|---|---|---|---|
| ATR | −9.6 | 88.0 | 0.29 | *** | 29.2 |
| CG | −10.5 | 56.1 | 0.20 | *** | 31.8 |
| CH | −5.2 | 23.7 | 0.10 | *** | 30.2 |
| CST | −3.3 | 18.9 | 0.08 | ** | 28.5 |
| Fmaj | −8.8 | 126.8 | 0.37 | *** | 24.5 |
| Fmin | −10.3 | 261.8 | 0.55 | *** | 24.0 |
| ILF | −8.0 | 102.4 | 0.32 | *** | 28.4 |
| SLF | −9.7 | 117.0 | 0.35 | *** | 28.8 |
| UF | −10.7 | 153.0 | 0.41 | *** | 28.6 |

Note: The FA values were computed as mean values in regions encompassing both the TBSS skeleton and the atlas-based tract. $t = t$ value, $F = F$ value, $R^2$ = adjusted $R^2$, age at maxima = age at LOESS estimated maximum FA. ATR: anterior thalamic radiation, CG: cingulum gyrus, CH: parahippocampal cingulate, CST: corticospinal tract, Fmaj: forceps major, Fmin: forceps minor, ILF: inferior longitudinal fasciculus, SLF: superior longitudinal fasciculus, UF: uncinate fasciculus. $^{**}P < 0.001$, $^{***}P < 0.0001$.

relationships with age. Median LOESS estimated maturational plateau for RD was 30.4 years (SD = 1.3) ranging from 29.1 years in Fmin to 32.7 years in the dorsal cingulum. Supplementary Figure 2 displays age × RD plots per hemisphere.

### *WM Volume*

Figure 3 shows age × WM volume plots for the various composite regions and Table 5 presents statistics from least-square regressions and age at LOESS estimated maxima. Standardized residual volumes after regressing out ICV and sex were used. All regions except the dorsal cingulum gyrus showed significant ($P < 0.05$, Bonferroni corrected) inverted U-shaped relationships with age. The dorsal cingulum gyrus showed a high degree of stability until the latest part of life. Median age at estimated peak for all areas was 52.2 years (SD = 8.0 years) ranging from 32.1 in corpus callosum to 55.9 years in the parietal lobe. Importantly, all regional WM volumes except corpus callosum peaked in the sixth decade.

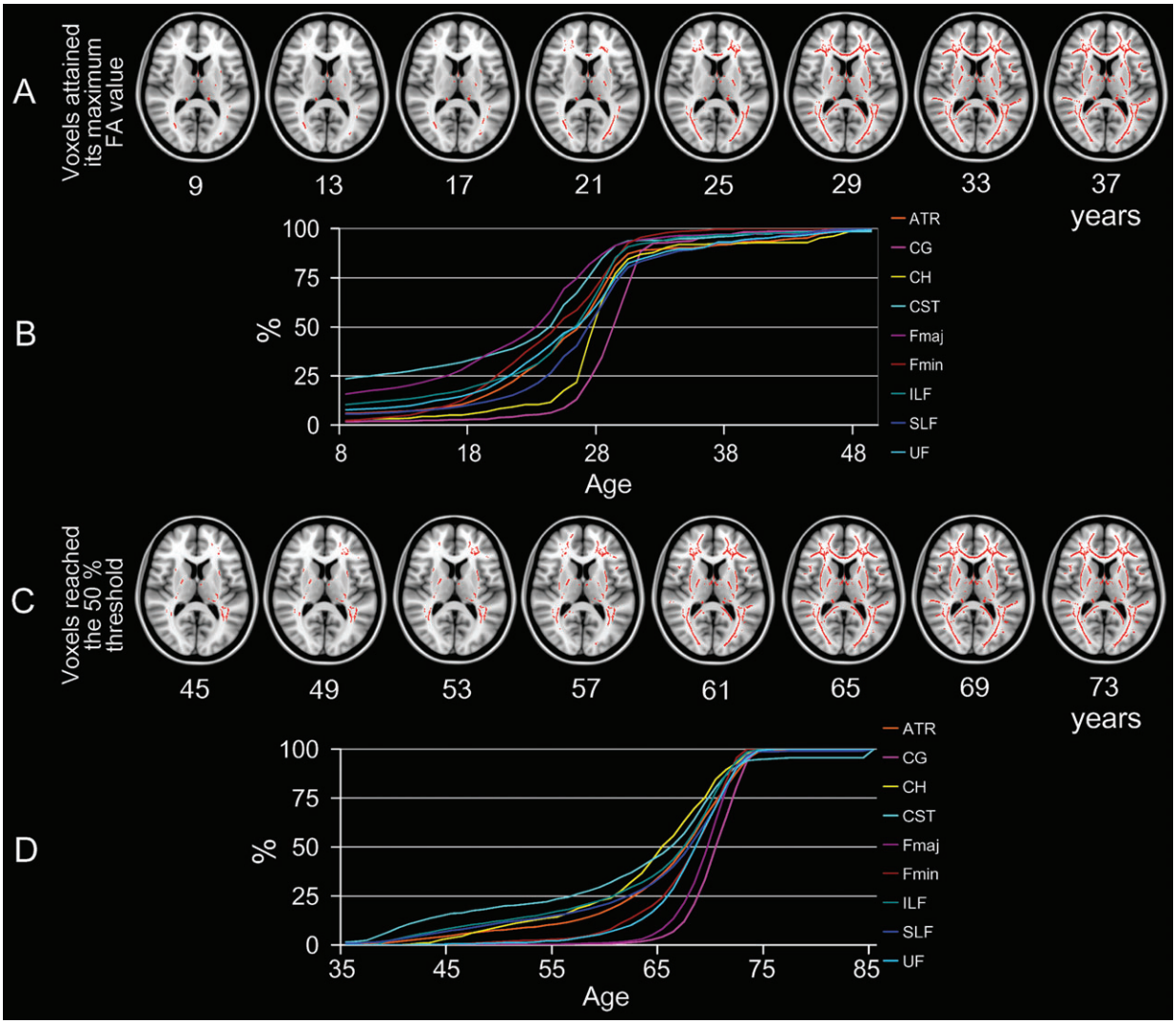


**Figure 6.** Regional variability in WM maturation and age-related deterioration. Panel *A* shows skeleton voxels (red) having attained its maximum rLOESS estimated FA value at different stages of chronological development in years. The skeleton voxels are superimposed on a transversal section of a T1-weighted Montreal Neurological Institute template ($Z = 83$). Only voxels showing a significant inverse U-pattern across the life span were included in the peak estimations. Relatively early maturation (<21 years) is seen in occipital and frontal areas. Panel *B* shows percentage of voxels per tract having reached its maximum FA value as a function of age (8–49 years). Panels *C* and *D* show the estimated age-related deterioration as indexed by age when FA fell below the value equal to 50% of the difference between maximum FA and FA at maximum age. Parts of the SLF reached the threshold at around 30 years of age, followed by areas encompassing Fmin in the late 40s and posterior areas, including the occipital lobes, in the early 60s. As indicated by the cumulative curves (panel *D*), the vast majority of voxels reached the threshold in the 60s.

## Discussion

Our analyses yielded several new findings. First, life-span age trajectories of FA, MD, and RD in WM are characterized by 3 phases: 1) a sharp developmental increase in FA and reduction in MD and RD followed by 2) a period of relative stability in adulthood with a subsequent 3) accelerated decrease in FA and increase in MD and RD in senescence. Second, the regional timing of maximum development for FA and RD was between 24 and 33 years, approximately 20 years earlier than the estimated peaks for WM volumes. Third, voxel-based fitting supported our hypothesis of relatively early maturation of the CST and slow development of the cingulum bundles. However, the regional variability did not provide ample evidence in support of a simple retrogenetic theory of age-related deterioration. Finally, the trajectories for WM volume and diffusion parameters were markedly different. Even though both were generally highly nonlinear, WM volumes increased until the sixth decade before starting to fall off. This stands in contrast to the much earlier plateaus observed for the DTI indices. We discuss the findings in more detail below.

U- or inverted U-shaped WM changes were found across modalities. This was not surprising given the inclusion of children. Total WM volume peaked at approximately 50 years of age, supporting the notion of WM volume growth until middle age (Jernigan et al. 2001; Allen et al. 2005; Fjell et al. 2005; Walhovd et al. forthcoming). However, global FA peaked at around 30 years followed by a small yet stable linear decrease until approximately 65 years with a subsequent accelerating decline. MD and RD showed analogous patterns. These trajectories do not support the notion of continuous WM maturation throughout large parts of adulthood, but rather suggest a 3-phasic life-span model with accelerated alterations

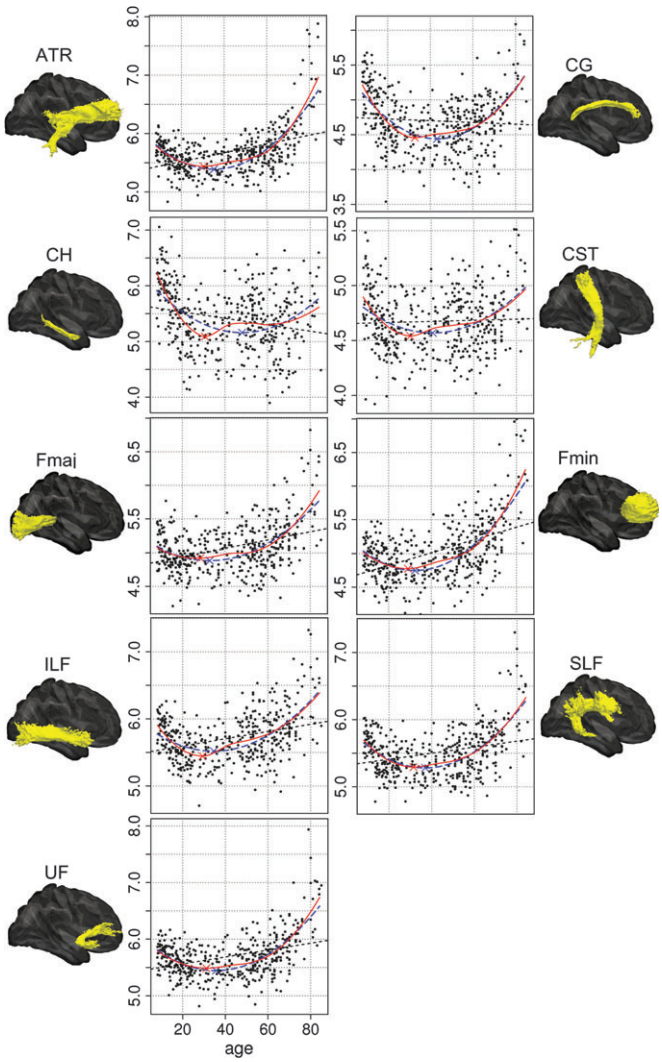


**Figure 7.** Regional RD through the life span. Individual mean RD ($10^{-4} \times mm^2/s$) from the various atlas tract × skeleton intersections plotted as a function of age. Black dotted lines denote the linear, blue lines the quadratic and red lines the LOESS fits. Blue and red crosses mark the estimated minima for the quadratic and LOESS fits, respectively. The yellow areas represent the probabilistically defined WM tracts used.

in the earliest and latest phases of life (Raz et al. 2005). This is further supported by developmental studies indicating an asymptotic WM maturation from childhood to early adulthood (Lebel et al. 2008; Østby et al. 2009; Tamnes et al. forthcoming) and accelerating WM volume decreases in senescence (Walhovd et al. forthcoming).

Tractwise estimation of the timing of maximum development showed relatively high regional stability, but some variability in the shape of the curves was observed. The volumetric data revealed a linear growth of frontal, parietal, and deep WM until estimated maxima, whereas the occipital and the cingulate WM remained relatively stable before declining in senescence. Thus, the continuous growth of total WM volume until peak was not representative for all areas. The DTI data showed a 3-phasic curve in the ATR, dorsal cingulum bundle, Fmin/Fmaj, inferior and superior longitudinal fasciculi and the uncinate. The uncinate trajectory is in general agreement with a recent DTI study (Hasan et al. 2009). The parahippocampal

**Table 4**
Results from OLS regressions with regional RD values as dependent and sex, age, and age$^2$ as independent variables

| RD | *t* | *F* | $R^2$ | sig | Age at minima (years) |
|---|---|---|---|---|---|
| ATR | 16.2 | 204.0 | 0.49 | *** | 30.4 |
| CG | 12.3 | 77.3 | 0.26 | *** | 32.7 |
| CH | 7.5 | 41.1 | 0.16 | *** | 30.7 |
| CST | 6.7 | 22.7 | 0.09 | ** | 30.2 |
| Fmaj | 8.8 | 78.1 | 0.26 | *** | 28.5 |
| Fmin | 12.2 | 159.3 | 0.43 | *** | 29.1 |
| ILF | 9.3 | 73.6 | 0.25 | *** | 29.3 |
| SLF | 12.8 | 106.8 | 0.33 | *** | 31.5 |
| UF | 13.4 | 135.1 | 0.39 | *** | 31.1 |

Note: The RD values were computed as mean values in regions encompassing both the TBSS skeleton and the atlas-based tract. $t = t$ value, $F = F$ value, $R^2$ = adjusted $R^2$, and age at minima = age at LOESS estimated minimum RD in the different tracts.
$^{**}P < 0.001$ and $^{***}P < 0.0001$.

**Table 5**
Results from OLS regressions with regional WM volumes as dependent and sex, age, and age$^2$ as independent variables

| | *t* | *F* | $R^2$ | sig | Age at maxima (years) |
|---|---|---|---|---|---|
| Deep WM | −11.6 | 81.0 | 0.27 | *** | 51.6 |
| Frontal WM | −6.9 | 25.9 | 0.10 | *** | 52.2 |
| Parietal WM | −6.5 | 24.2 | 0.10 | *** | 55.9 |
| Occipital WM | −3.1 | 4.9 | 0.02 | ** | 52.4 |
| Temporal WM | −7.0 | 24.7 | 0.10 | *** | 52.7 |
| Cingulate WM | −2.5 | 6.0 | 0.02 | n.s. | 52.1 |
| Corpus Callosum WM | −8.6 | 69.2 | 0.24 | *** | 32.1 |

Note: All volumes are residuals after regressing out ICV. $t = t$ value, $F = F$ value, $R^2$ = adjusted $R^2$, and age at maxima = age at LOESS estimated maximum volumes.
*n.s: not significant; $^{**}P < 0.001$ and $^{***}P < 0.0001$.

cingulum showed a less clear-cut trajectory. Steepest developmental curves were seen in the dorsal cingulum bundle. Because we sampled from 8 years of age, this is probably indicative of prolonged maturation of the dorsal cingulum, which is in line with previous reports (Lebel et al. 2008; Tamnes et al. forthcoming). The voxel-based fitting yielded results supporting our hypothesis of early maturation of the CST and protracted development in the dorsal and parahippocampal cingulum bundles. However, the relatively late deterioration observed in the dorsal cingulum bundles and the uncinate does not support a simple retrogenetic theory of WM deterioration in aging.

The neurobiological mechanisms causing volumetric and diffusivity changes in brain tissue in development and aging are not understood. Findings from comparative and histological studies suggest significant alterations of myelin-related processes in aging (Peters 2002a), including accumulation of water-containing balloons in the myelin sheaths (Feldman and Peters 1998; Sugiyama et al. 2002), formation of redundant myelin, splitting of the myelin lamellae and loss of small myelinated nerve fibers (Sandell and Peters 2001, 2003; Marner et al. 2003). Also, evidence of increased number of oligodendrocytes (Peters and Sethares 2004), thickening of myelin lamellae (Peters et al. 2001), and shortening of the internodes (Peters and Sethares 2003) in aged subjects is indicative of remyelination in old age (Lasiene et al. 2009). Other factors influencing both volume and diffusion measures include alterations of the fiber diameter (Paus et al. 2008; Giorgio et al. 2010). Several environmental and

experiential variables influence WM development (Bengtsson et al. 2005; Fields 2008; Hyde et al. 2009); thus, life-span WM changes manifest through a dynamic pattern of neurobiological and environmental interactions.

The most apparent discrepancy between measures was the age at estimated maximum development; with a span of more than 20 years between estimated global FA (29.1 years) and total WM volume peak (50.1 years). The early DTI maturational maxima are not in accordance with previous volumetric studies, and do not lend support for WM development beyond early adulthood. There were small regional differences in WM volume peaks, and all regions peaked early in the sixth decade with the exception of corpus callosum, which peaked in the beginning of the thirties. Tract-specific analyses for FA and RD showed maximum development late in the third or early in the fourth decade in all tracts. One exception was the parahippocampal cingulum bundles, which showed less clear trajectories. This is in accordance with a previous study failing to find age-related FA decrease in the temporal lobe (Hsu et al. 2008).

The voxel-based rLOESS procedure revealed relatively early maturation of not only occipital areas (~15–20 years) but also frontal areas including portions of the Fmin that reached maximum FA value in late teen years. The cumulative tractwise maturational curves (Fig. 6, panel *B*) indicated relatively small differences in the timing of maturation between tracts. Some interesting exceptions are noted. For Fmaj and CST, 50% of the voxels peaked around 20 years of age, whereas the parahippocampal (~27 years) and the dorsal cingulum bundles (~30 years) showed a slower maturation. This is in line with our hypothesis of protracted development in fronto-temporal connections. Interestingly, Fmaj and the dorsal cingulum bundles were among the latest tracts to deteriorate as indexed by the 50% threshold (Fig. 6, panel *D*), whereas the CST was among the earliest. This does not support our hypothesis of an inversed ontogenetic pattern in WM aging. As indicated by the tractwise smoothing, most voxels peaked within 30 years of age. The voxel-based rLOESS analyses of age-related WM deterioration showed that parts of the SLF reached the 50% threshold already at around 30 years of age, followed by parts of the Fmin in the late 40s and more posterior areas in the early 60s. As indicated by the cumulative curves, most voxels reached the threshold between 55 and 65 years of age.

A critical question pertaining to the neuroanatomical inferences of the regional differences is to which degree DTI indices are sensitive to between regions compared with between subjects variability. Mädler et al. (2008) reported a correlation between FA/RD and myelin water fraction (MWF, based on the short T2 component) across but not within regions. With a few exceptions, the lack of a clear tractwise segregation in developmental sequence and also the strong correlations between tracts in our data, suggest that DTI indices may be more sensitive to global than to regional variability in neurodevelopment and aging. Thus, neuroanatomical inferences based on DTI indices alone should be made with caution.

Our results suggest that tissue volume and DTI measures are relatively independent indices of WM properties. Although the volumetric data indicate a 2-phasic development with an initial growth until middle age followed by accelerated loss, the DTI data showed earlier maximum maturation followed by a relatively stable and slow decline until late middle life with an accelerating decline in senescence. Few MRI studies have examined concurrent volume and diffusion changes across the brain. Hugenschmidt et al. (2008) reported age-related FA decreases in subjects aged 18–80 years after correcting for local atrophy as indexed by decreased WM volume. This supports the notion that FA is sensitive to microstructural changes preceding tissue loss. Abe et al. (2008) found regional selectivity for age-related FA and volume changes, respectively, indicating that the measures are complementary neurobiological markers. The relative independence of DTI and volumetry as indices of cerebral health is also supported by findings of weak associations between the 2 measures (Fjell et al. 2008). One study reported that age-related decreases in FA could primarily be explained by atrophy and lesion formation (Vernooij et al. 2008). However, the sample was restricted to subjects above 60 years of age, approximately 30 years after estimated maximum FA in our data. Although pathological mechanisms like lesion formations and tissue atrophy may partly explain individual differences in FA in elderly subjects, such pathological factors exert minimal influence in healthy young subjects. Thus, the mechanisms involved in FA reduction in young versus old adulthood may be fundamentally different.

We have earlier speculated that formation of redundant myelin and water compartments in the myelin sheaths may increase volume and decrease FA, and thus exert differential age effects on the 2 measures (Fjell et al. 2008). However, DTI indices are sensitive to general diffusion properties of brain tissue, and are not a selective marker of myelin (Beaulieu 2002). Nevertheless, the magnitude of the radial eigenvalue has been shown to be sensitive to de- and dysmyelination in mice (Song et al. 2002, 2005), suggesting some myelin specificity of RD. Also, histological analyses indicate FA and MD sensitivity to myelin content, and to a lesser degree axonal count (Schmierer et al. 2007). The estimated maturational peaks of the DTI indices suggest that some developmental processes influencing WM diffusivity halt or reverse in the fourth decade. The DTI data thus contradict the notion of positive WM development until middle age. Although attributing the timing of the maturational DTI maxima to myelin-related neurobiological processes may be tempting, the present findings must also be interpreted in light of evidence of continued remodeling of the myelin until the sixth decade (Flynn et al. 2003; Inglese and Ge 2004).

### *Limitations*

Our study has several limitations. Possible confounds in cross-sectional studies include cohort effects, such as nutrition/dietary patterns during gestation and early development. Profiting from longitudinal data, further studies would also be able to validate the current cross-sectional curves with individual trajectories of both diffusivity and volumetric measures. Follow-up assessments of the included participants are planned.

Another potential limitation is that the diffusion data were derived exclusively from the center of each pathway. It has been suggested that thin myelinated fibers more proximal to the brain surface or in the periphery of the fasciculi may be more vulnerable to age-related degradation than deeper structures (Sandell and Peters 2001, 2003; Marner et al. 2003; Bartzokis 2004). Thus, the sampled neuroanatomical regions may not be optimal in order to explore the proposed

last-in-first-out hypothesis of cerebral aging, as actively myelinating areas closer to the cortical surface may show different maturational and aging-related patterns (Bartzokis 2004). Due to constraints on image resolution in DTI and many crossing fibers close to the cortical mantle, DTI data supporting this hypothesis is lacking, and more studies utilizing other modalities with superior resolution are needed (Salat, Lee, et al. 2009; Westlye, Walhovd, Dale, et al. 2009). Recent techniques for modeling and separating multiple crossing fiber populations (Jbabdi et al. 2010) and identifying the entire extent of specific WM tracts (Hagler et al. 2009) based on DTI scans may provide tract-specific diffusion estimates that overcome this limitation.

A challenge in imaging studies comparing participants with possibly different macrostructural brain characteristics is that different amounts of warping to standard space are needed. In the present study, FNIRT performed the native-to-standard space warping adequately across age groups. As a global comparison was the main reason for inclusion of multimodal data, the methodological approach employed did not enable a direct local comparison of WM volume and DTI indices.

The included participants showed generally above average cognitive functioning, and may thus not be representative for the general population. This is a shortcoming of many studies aiming at pinpointing healthy aging (Raz et al. 2005). Also, despite our efforts to include healthy participants only in the current sample, including health interview, cognitive assessments and radiological evaluation, the influence of subclinical conditions on the measures of interest cannot be ruled out. As neurodegenerative conditions may be manifested in the brain years before clinical symptoms are detectable, follow-up examinations over several years are needed to exclude the possibility that, for example, preclinical AD may have influenced the results. We did not exclude areas showing subtle T2-weighted WM hyperintensities from the DTI analyses. Thus, we cannot rule out a possible influence of subclinical conditions affecting T1- or T2-weighted signal intensities on the DTI indices. However, signal intensity alterations are regularly found in healthy samples, and may not be a specific neuroradiological marker of disease (Vernooij et al. 2007). Further, reductions in FA were seen from about 30 years of age, and it is unlikely that preclinical AD or other incipient neurodegenerative conditions cause WM changes at this age.

## Conclusion

The present results demonstrated that microstructural WM maturation peaks early in the fourth decade, with no evidence of protracted development into middle age. The time-lapse sequences supported early maturation of occipital areas and the CSTs but did not provide ample evidence in support of a simple last-in-first-out hypothesis, nor any strong indication of a selective vulnerability of the frontal lobes in aging. The estimated DTI trajectories supported a 3-phasic life-span model with accelerating alterations in the earliest and latest part of life with an intermediate slow decline from early adulthood into middle age (Raz et al. 2005). The timing of the DTI maturational plateaus, estimated to be in the early 30s, were markedly earlier than for WM volumes, which in general were characterized by quadratic trajectories with peaks in the early 50s. Still, both the DTI and the volumetry trajectories diverge from what is usually observed for cortical volume and thickness, which in general follows a monotonic pattern of reduction throughout most of adolescence and adulthood.

## Supplementary Material

Supplementary material can be found at: http://www.cercor.oxfordjournals.org/.

## Funding

Norwegian Research Council (grant 177404/W50 to K.B.W. and 175066/D15 to A.M.F.) and University of Oslo to K.B.W. and A.M.F.

## Notes

*Conflict of Interest*: Anders M. Dale is a founder and holds equity in CorTechs Labs, Inc, and also serves on the Scientific Advisory Board. The terms of this arrangement have been reviewed and approved by the University of California, San Diego, in accordance with its conflict of interest policies. All other authors state that there are no actual or potential conflicts of interest.

Address correspondence to Lars Tjelta Westlye, Department of Psychology, Center for the Study of Human Cognition, University of Oslo, PO Box 1094, Blindern 0317, Oslo, Norway. Email: l.t.westlye@psykologi.uio.no.

## References

Abe O, Yamasue H, Aoki S, Suga M, Yamada H, Kasai K, Masutani Y, Kato N, Ohtomo K. 2008. Aging in the CNS: comparison of gray/white matter volume and diffusion tensor data. Neurobiol Aging. 29:102–116.

Allen JS, Bruss J, Brown CK, Damasio H. 2005. Normal neuroanatomical variation due to age: the major lobes and a parcellation of the temporal region. Neurobiol Aging. 26:1245–1260;discussion 1279–1282.

Andersson JLR, Jenkinson M, Smith S. 2007a. Non-linear optimisation. In: FMRIB technical report TR07JA1 from www.fmrib.ox.ac.uk/analysis/techrep.

Andersson JLR, Jenkinson M, Smith S. 2007b. Non-linear registration, aka Spatial normalisation. In: FMRIB technical report TR07JA2 from www.fmrib.ox.ac.uk/analysis/techrep.

Ardekani S, Kumar A, Bartzokis G, Sinha U. 2007. Exploratory voxel-based analysis of diffusion indices and hemispheric asymmetry in normal aging. Magn Reson Imaging. 25:154–167.

Ashtari M, Cervellione KL, Hasan KM, Wu J, McIlree C, Kester H, Ardekani BA, Roofeh D, Szeszko PR, Kumra S. 2007. White matter development during late adolescence in healthy males: a cross-sectional diffusion tensor imaging study. Neuroimage. 35:501–510.

Bartzokis G. 2004. Age-related myelin breakdown: a developmental model of cognitive decline and Alzheimer's disease. Neurobiol Aging. 25:5–18. author reply 49–62.

Bartzokis G, Beckson M, Lu PH, Nuechterlein KH, Edwards N, Mintz J. 2001. Age-related changes in frontal and temporal lobe volumes in men: a magnetic resonance imaging study. Arch Gen Psychiatry. 58:461–465.

Beaulieu C. 2002. The basis of anisotropic water diffusion in the nervous system - a technical review. NMR Biomed. 15:435–455.

Beck AT, Steer R. 1987. Beck Depression Inventory Scoring manual. New York: The Psychological Corporation.

Bengtsson SL, Nagy Z, Skare S, Forsman L, Forssberg H, Ullen F. 2005. Extensive piano practicing has regionally specific effects on white matter development. Nat Neurosci. 8:1148–1150.

Bravo G, Hebert R. 1997. Age- and education-specific reference values for the Mini-Mental and modified Mini-Mental State Examinations derived from a non-demented elderly population. Int J Geriatr Psychiatry. 12:1008–1018.

Buckner RL, Head D, Parker J, Fotenos AF, Marcus D, Morris JC, Snyder AZ. 2004. A unified approach for morphometric and

functional data analysis in young, old, and demented adults using automated atlas-based head size normalization: reliability and validation against manual measurement of total intracranial volume. Neuroimage. 23:724–738.
Charlton RA, Barrick TR, McIntyre DJ, Shen Y, O'Sullivan M, Howe FA, Clark CA, Morris RG, Markus HS. 2006. White matter damage on diffusion tensor imaging correlates with age-related cognitive decline. Neurology. 66:217–222.
Cleveland WS, Devlin SJ. 1988. Locally weighted regression: an approach to regression analysis by local ditting. J Am Stat Assoc. 83:596–610.
Courchesne E, Chisum HJ, Townsend J, Cowles A, Covington J, Egaas B, Harwood M, Hinds S, Press GA. 2000. Normal brain development and aging: quantitative analysis at in vivo MR imaging in healthy volunteers. Radiology. 216:672–682.
Dale AM, Fischl B, Sereno MI. 1999. Cortical surface-based analysis. I. Segmentation and surface reconstruction. Neuroimage. 9:179–194.
Davis SW, Dennis NA, Buchler NG, White LE, Madden DJ, Cabeza R. 2009. Assessing the effects of age on long white matter tracts using diffusion tensor tractography. Neuroimage. 46:530–541.
Desikan RS, Segonne F, Fischl B, Quinn BT, Dickerson BC, Blacker D, Buckner RL, Dale AM, Maguire RP, Hyman BT, et al. 2006. An automated labeling system for subdividing the human cerebral cortex on MRI scans into gyral based regions of interest. Neuroimage. 31:968–980.
Feldman ML, Peters A. 1998. Ballooning of myelin sheaths in normally aged macaques. J Neurocytol. 27:605–614.
Fields RD. 2008. White matter in learning, cognition and psychiatric disorders. Trends Neurosci. 31:361–370.
Fischl B, Dale AM. 2000. Measuring the thickness of the human cerebral cortex from magnetic resonance images. Proc Natl Acad Sci U S A. 97:11050–11055.
Fischl B, Liu A, Dale AM. 2001. Automated manifold surgery: constructing geometrically accurate and topologically correct models of the human cerebral cortex. IEEE Trans Med Imaging. 20:70–80.
Fischl B, Sereno MI, Dale AM. 1999. Cortical surface-based analysis. II: inflation, flattening, and a surface-based coordinate system. Neuroimage. 9:195–207.
Fischl B, Sereno MI, Tootell RB, Dale AM. 1999. High-resolution intersubject averaging and a coordinate system for the cortical surface. Hum Brain Mapp. 8:272–284.
Fischl B, van der Kouwe A, Destrieux C, Halgren E, Segonne F, Salat DH, Busa E, Seidman LJ, Goldstein J, Kennedy D, et al. 2004. Automatically parcellating the human cerebral cortex. Cereb Cortex. 14:11–22.
Fjell AM, Walhovd KB, Reinvang I, Lundervold A, Dale AM, Quinn BT, Makris N, Fischl B. 2005. Age does not increase rate of forgetting over weeks–neuroanatomical volumes and visual memory across the adult life-span. J Int Neuropsychol Soc. 11:2–15.
Fjell AM, Westlye LT, Greve DN, Fischl B, Benner T, van der Kouwe AJ, Salat D, Bjørnerud A, Due-Tønnessen P, Walhovd KB. 2008. The relationship between diffusion tensor imaging and volumetry as measures of white matter properties. Neuroimage. 42: 1654–1668.
Flynn SW, Lang DJ, Mackay AL, Goghari V, Vavasour IM, Whittall KP, Smith GN, Arango V, Mann JJ, Dwork AJ, et al. 2003. Abnormalities of myelination in schizophrenia detected in vivo with MRI, and post-mortem with analysis of oligodendrocyte proteins. Mol Psychiatry. 8:811–820.
Folstein MF, Folstein SE, McHugh PR. 1975. Mini-mental state". A practical method for grading the cognitive state of patients for the clinician. J Psychiatr Res. 12:189–198.
Fotenos AF, Snyder AZ, Girton LE, Morris JC, Buckner RL. 2005. Normative estimates of cross-sectional and longitudinal brain volume decline in aging and AD. Neurology. 64:1032–1039.
Giedd JN, Blumenthal J, Jeffries NO, Castellanos FX, Liu H, Zijdenbos A, Paus T, Evans AC, Rapoport JL. 1999. Brain development during childhood and adolescence: a longitudinal MRI study. Nat Neurosci. 2:861–863.
Giorgio A, Watkins KE, Chadwick M, James S, Winmill L, Douaud G, De Stefano N, Matthews PM, Smith SM, Johansen-Berg H, et al. 2010. Longitudinal changes in grey and white matter during adolescence. Neuroimage. 49:94–103.
Giorgio A, Watkins KE, Douaud G, James AC, James S, De Stefano N, Matthews PM, Smith SM, Johansen-Berg H. 2008. Changes in white matter microstructure during adolescence. Neuroimage. 39:52–61.
Grieve SM, Williams LM, Paul RH, Clark CR, Gordon E. 2007. Cognitive aging, executive function, and fractional anisotropy: a diffusion tensor MR imaging study. AJNR Am J Neuroradiol. 28:226–235.
Hagler DJ, Jr., Ahmadi ME, Kuperman J, Holland D, McDonald CR, Halgren E, Dale AM. 2009. Automated white-matter tractography using a probabilistic diffusion tensor atlas: application to temporal lobe epilepsy. Hum Brain Mapp. 30:1535–1547.
Hasan KM, Iftikhar A, Kamali A, Kramer LA, Ashtari M, Cirino PT, Papanicolaou AC, Fletcher JM, Ewing-Cobbs L. 2009. Development and aging of the healthy human brain uncinate fasciculus across the lifespan using diffusion tensor tractography. Brain Res. 18:67–76.
Hasan KM, Sankar A, Halphen C, Kramer LA, Brandt ME, Juranek J, Cirino PT, Fletcher JM, Papanicolaou AC, Ewing-Cobbs L. 2007. Development and organization of the human brain tissue compartments across the lifespan using diffusion tensor imaging. Neuroreport. 18:1735–1739.
Head D, Buckner RL, Shimony JS, Williams LE, Akbudak E, Conturo TE, McAvoy M, Morris JC, Snyder AZ. 2004. Differential vulnerability of anterior white matter in nondemented aging with minimal acceleration in dementia of the Alzheimer type: evidence from diffusion tensor imaging. Cereb Cortex. 14:410–423.
Hsu JL, Leemans A, Bai CH, Lee CH, Tsai YF, Chiu HC, Chen WH. 2008. Gender differences and age-related white matter changes of the human brain: a diffusion tensor imaging study. Neuroimage. 39:566–577.
Hua K, Zhang J, Wakana S, Jiang H, Li X, Reich DS, Calabresi PA, Pekar JJ, van Zijl PC, Mori S. 2008. Tract probability maps in stereotaxic spaces: analyses of white matter anatomy and tract-specific quantification. Neuroimage. 39:336–347.
Hugenschmidt CE, Peiffer AM, Kraft RA, Casanova R, Deibler AR, Burdette JH, Maldjian JA, Laurienti PJ. 2008. Relating imaging indices of white matter integrity and volume in healthy older adults. Cereb Cortex. 18:433–442.
Hyde KL, Lerch J, Norton A, Forgeard M, Winner E, Evans AC, Schlaug G. 2009. Musical training shapes structural brain development. J Neurosci. 29:3019–3025.
Ikram MA, Vrooman HA, Vernooij MW, van der Lijn F, Hofman A, van der Lugt A, Niessen WJ, Breteler MM. 2008. Brain tissue volumes in the general elderly population. The Rotterdam Scan Study. Neurobiol Aging. 29:882–890.
Inglese M, Ge Y. 2004. Quantitative MRI: hidden age-related changes in brain tissue. Top Magn Reson Imaging. 15:355–363.
Jbabdi S, Behrens TE, Smith SM. 2010. Crossing fibres in tract-based spatial statistics. Neuroimage. 49:249–256.
Jenkinson M, Smith S. 2001. A global optimisation method for robust affine registration of brain images. Med Image Anal. 5:143–156.
Jernigan TL, Archibald SL, Fennema-Notestine C, Gamst AC, Stout JC, Bonner J, Hesselink JR. 2001. Effects of age on tissues and regions of the cerebrum and cerebellum. Neurobiol Aging. 22:581–594.
Kennedy KM, Raz N. 2009a. Aging white matter and cognition: differential effects of regional variations in diffusion properties on memory, executive functions, and speed. Neuropsychologia. 47:916–927.
Kennedy KM, Raz N. 2009b. Pattern of normal age-related regional differences in white matter microstructure is modified by vascular risk. Brain Res. 1297:41–56.
Kinney HC, Brody BA, Kloman AS, Gilles FH. 1988. Sequence of central nervous system myelination in human infancy. II. Patterns of myelination in autopsied infants. J Neuropathol Exp Neurol. 47:217–234.
Klingberg T, Vaidya CJ, Gabrieli JD, Moseley ME, Hedehus M. 1999. Myelination and organization of the frontal white matter in children: a diffusion tensor MRI study. Neuroreport. 10:2817–2821.

Kochunov P, Thompson PM, Lancaster JL, Bartzokis G, Smith S, Coyle T, Royall DR, Laird A, Fox PT. 2007. Relationship between white matter fractional anisotropy and other indices of cerebral health in normal aging: tract-based spatial statistics study of aging. Neuroimage. 35:478–487.

Lasiene J, Matsui A, Sawa Y, Wong F, Horner PJ. 2009. Age-related myelin dynamics revealed by increased oligodendrogenesis and short internodes. Aging Cell. 8:201–213.

Le Bihan D. 2003. Looking into the functional architecture of the brain with diffusion MRI. Nat Neurosci. 4:469–480.

Lebel C, Walker L, Leemans A, Phillips L, Beaulieu C. 2008. Microstructural maturation of the human brain from childhood to adulthood. Neuroimage. 40:1044–1055.

Lenroot RK, Gogtay N, Greenstein DK, Wells EM, Wallace GL, Clasen LS, Blumenthal JD, Lerch J, Zijdenbos AP, Evans AC, et al. 2007. Sexual dimorphism of brain developmental trajectories during childhood and adolescence. Neuroimage. 36:1065–1073.

Liston C, Watts R, Tottenham N, Davidson MC, Niogi S, Ulug AM, Casey BJ. 2006. Frontostriatal microstructure modulates efficient recruitment of cognitive control. Cereb Cortex. 16:553–560.

Mädler B, Drabycz SA, Kolind SH, Whittall KP, MacKay AL. 2008. Is diffusion anisotropy an accurate monitor of myelination? Correlation of multicomponent T2 relaxation and diffusion tensor anisotropy in human brain. Magn Reson Imaging. 26:874–888.

Marner L, Nyengaard JR, Tang Y, Pakkenberg B. 2003. Marked loss of myelinated nerve fibers in the human brain with age. J Comp Neurol. 462:144–152.

Mori S, Wakana S, van Zijl PCM, Nagae-Poetscher LM. 2005. MRI atlas of human white matter. Amsterdam (Netherlands): Elsevier.

Nichols TE, Holmes AP. 2002. Nonparametric permutation tests for functional neuroimaging: a primer with examples. Hum Brain Mapp. 15:1–25.

Olesen PJ, Nagy Z, Westerberg H, Klingberg T. 2003. Combined analysis of DTI and fMRI data reveals a joint maturation of white and grey matter in a fronto-parietal network. Brain Res Cogn Brain Res. 18:48–57.

O'Sullivan M, Jones DK, Summers PE, Morris RG, Williams SC, Markus HS. 2001. Evidence for cortical "disconnection" as a mechanism of age-related cognitive decline. Neurology. 57:632–638.

Østby Y, Tamnes CK, Fjell AM, Westlye LT, Due-Tønnessen P, Walhovd KB. 2009. Heterogeneity in subcortical brain development: a structural MRI study of brain maturation from 8-30 years. J Neurosci. 29:11772–11782.

Paus T, Keshavan M, Giedd JN. 2008. Why do many psychiatric disorders emerge during adolescence? Nat Rev Neurosci. 9:947–957.

Paus T, Zijdenbos A, Worsley K, Collins DL, Blumenthal J, Giedd JN, Rapoport JL, Evans AC. 1999. Structural maturation of neural pathways in children and adolescents: in vivo study. Science. 283:1908–1911.

Perry ME, McDonald CR, Hagler DJ, Jr, Gharapetian L, Kuperman JM, Koyama AK, Dale AM, McEvoy LK. 2009. White matter tracts associated with set-shifting in healthy aging. Neuropsychologia. 47:2835–2842.

Peters A. 2002a. The effects of normal aging on myelin and nerve fibers: a review. J Neurocytol. 31:581–593.

Peters A. 2002b. Structural changes that occur during normal aging of primate cerebral hemispheres. Neurosci Biobehav Rev. 26: 733–741.

Peters A, Sethares C. 2003. Is there remyelination during aging of the primate central nervous system? J Comp Neurol. 460:238–254.

Peters A, Sethares C. 2004. Oligodendrocytes, their progenitors and other neuroglial cells in the aging primate cerebral cortex. Cereb Cortex. 14:995–1007.

Peters A, Sethares C, Killiany RJ. 2001. Effects of age on the thickness of myelin sheaths in monkey primary visual cortex. J Comp Neurol. 435:241–248.

Pfefferbaum A, Adalsteinsson E, Sullivan EV. 2005. Frontal circuitry degradation marks healthy adult aging: evidence from diffusion tensor imaging. Neuroimage. 26:891–899.

Pierpaoli C, Basser PJ. 1996. Toward a quantitative assessment of diffusion anisotropy. Magn Reson Med. 36:893–906.

Raz N. 2000. Aging of the brain and its impact on cognitive performance: integration of structural and functional findings. In: Craik FIM, Salthouse TA, editors. Handbook of aging and cognition—II. Mahwah (NJ): Erlbaum. p. 1–90.

Raz N, Gunning-Dixon F, Head D, Rodrigue KM, Williamson A, Acker JD. 2004. Aging, sexual dimorphism, and hemispheric asymmetry of the cerebral cortex: replicability of regional differences in volume. Neurobiol Aging. 25:377–396.

Raz N, Kennedy KM. 2009. A systems approach to age-related change: neuroanatomical changes, their modifiers, and cognitive correlates. In: Jagust WJ, D'Esposito M, editors. Imaging the aging brain. New York: Oxford University Press. p. 43–70.

Raz N, Lindenberger U, Rodrigue KM, Kennedy KM, Head D, Williamson A, Dahle C, Gerstorf D, Acker JD. 2005. Regional brain changes in aging healthy adults: general trends, individual differences and modifiers. Cereb Cortex. 15:1676–1689.

Reese TG, Heid O, Weisskoff RM, Wedeen VJ. 2003. Reduction of eddy-current-induced distortion in diffusion MRI using a twice-refocused spin echo. Magn Reson Med. 49:177–182.

Resnick SM, Pham DL, Kraut MA, Zonderman AB, Davatzikos C. 2003. Longitudinal magnetic resonance imaging studies of older adults: a shrinking brain. J Neurosci. 23:3295–3301.

Rueckert D, Sonoda LI, Hayes C, Hill DL, Leach MO, Hawkes DJ. 1999. Nonrigid registration using free-form deformations: application to breast MR images. IEEE Trans Med Imaging. 18:712–721.

Salat DH, Greve DN, Pacheco JL, Quinn BT, Helmer KG, Buckner RL, Fischl B. 2009. Regional white matter volume differences in nondemented aging and Alzheimer's disease. Neuroimage. 44:1247–1258.

Salat DH, Lee SY, van der Kouwe AJ, Greve DN, Fischl B, Rosas HD. 2009. Age-associated alterations in cortical gray and white matter signal intensity and gray to white matter contrast. Neuroimage. 48:21–28.

Salat DH, Tuch DS, Greve DN, van der Kouwe AJ, Hevelone ND, Zaleta AK, Rosen BR, Fischl B, Corkin S, Rosas HD, et al. 2005. Age-related alterations in white matter microstructure measured by diffusion tensor imaging. Neurobiol Aging. 26:1215–1227.

Salat DH, Tuch DS, Hevelone ND, Fischl B, Corkin S, Rosas HD, Dale AM. 2005. Age-related changes in prefrontal white matter measured by diffusion tensor imaging. Ann N Y Acad Sci. 1064:37–49.

Salat DH, Tuch DS, van der Kouwe AJ, Greve DN, Pappu V, Lee SY, Hevelone ND, Zaleta AK, Growdon JH, Corkin S. Forthcoming. White matter pathology isolates the hippocampal formation in Alzheimer's disease. Neurobiol Aging. doi: 10.1016/j.neurobiolaging.2008.03.013.

Sandell JH, Peters A. 2001. Effects of age on nerve fibers in the rhesus monkey optic nerve. J Comp Neurol. 429:541–553.

Sandell JH, Peters A. 2003. Disrupted myelin and axon loss in the anterior commissure of the aged rhesus monkey. J Comp Neurol. 466:14–30.

Schmierer K, Wheeler-Kingshott CA, Boulby PA, Scaravilli F, Altmann DR, Barker GJ, Tofts PS, Miller DH. 2007. Diffusion tensor imaging of post mortem multiple sclerosis brain. Neuroimage. 35:467–477.

Segonne F, Dale AM, Busa E, Glessner M, Salat D, Hahn HK, Fischl B. 2004. A hybrid approach to the skull stripping problem in MRI. Neuroimage. 22:1060–1075.

Smith SM. 2002. Fast robust automated brain extraction. Hum Brain Mapp. 17:143–155.

Smith SM, Jenkinson M, Johansen-Berg H, Rueckert D, Nichols TE, Mackay CE, Watkins KE, Ciccarelli O, Cader MZ, Matthews PM, et al. 2006. Tract-based spatial statistics: voxelwise analysis of multi-subject diffusion data. Neuroimage. 31:1487–1505.

Smith SM, Jenkinson M, Woolrich MW, Beckmann CF, Behrens TE, Johansen-Berg H, Bannister PR, De Luca M, Drobnjak I, Flitney DE, et al. 2004. Advances in functional and structural MR image analysis and implementation as FSL. Neuroimage. 23(Suppl. 1): S208–S219.

Smith SM, Johansen-Berg H, Jenkinson M, Rueckert D, Nichols TE, Miller KL, Robson MD, Jones DK, Klein JC, Bartsch AJ, et al. 2007. Acquisition and voxelwise analysis of multi-subject diffusion data with tract-based spatial statistics. Nat Protoc. 2:499–503.

Smith SM, Nichols TE. 2009. Threshold-free cluster enhancement: addressing problems of smoothing, threshold dependence and localisation in cluster inference. Neuroimage. 44:83–98.
Song SK, Sun SW, Ramsbottom MJ, Chang C, Russell J, Cross AH. 2002. Dysmyelination revealed through MRI as increased radial (but unchanged axial) diffusion of water. Neuroimage. 17: 1429–1436.
Song SK, Yoshino J, Le TQ, Lin SJ, Sun SW, Cross AH, Armstrong RC. 2005. Demyelination increases radial diffusivity in corpus callosum of mouse brain. Neuroimage. 26:132–140.
Sugiyama I, Tanaka K, Akita M, Yoshida K, Kawase T, Asou H. 2002. Ultrastructural analysis of the paranodal junction of myelinated fibers in 31-month-old-rats. J Neurosci Res. 70:309–317.
Sullivan EV, Pfefferbaum A. 2006. Diffusion tensor imaging and aging. Neurosci Biobehav Rev. 30:749–761.
Tamnes CK, Østby Y, Fjell AM, Westlye LT, Due-Tønnessen P, Walhovd KB. Forthcoming Brain maturation in adolescence and young adulthood: regional age-related changes in cortical thickness and white matter volume and microstructure. Cereb Cortex.
Tang Y, Nyengaard JR, Pakkenberg B, Gundersen HJ. 1997. Age-induced white matter changes in the human brain: a stereological investigation. Neurobiol Aging. 18:609–615.
Tuch DS, Salat DH, Wisco JJ, Zaleta AK, Hevelone ND, Rosas HD. 2005. Choice reaction time performance correlates with diffusion anisotropy in white matter pathways supporting visuospatial attention. Proc Natl Acad Sci U S A. 102:12212–12217.
Vernooij MW, de Groot M, van der Lugt A, Ikram MA, Krestin GP, Hofman A, Niessen WJ, Breteler MM. 2008. White matter atrophy and lesion formation explain the loss of structural integrity of white matter in aging. Neuroimage. 43:470–477.
Vernooij MW, Ikram MA, Tanghe HL, Vincent AJ, Hofman A, Krestin GP, Niessen WJ, Breteler MM, van der Lugt A. 2007. Incidental findings on brain MRI in the general population. N Engl J Med. 357:1821–1828.
Wakana S, Jiang H, Nagae-Poetscher LM, van Zijl PC, Mori S. 2004. Fiber tract-based atlas of human white matter anatomy. Radiology. 230:77–87.
Walhovd KB, Westlye LT, Amlien I, Espeseth T, Reinvang I, Raz N, Agartz I, Salat D, Greve DN, Fischl B, et al. Forthcoming. Consistent neuroanatomical age-related volume differences across multiple samples. Neurobiol Aging.
Wechsler D. 1999. Wechsler Abbreviated Scale of Intelligence. San Antonio (TX): The Psychological Corporation.
Westlye LT, Walhovd KB, Bjørnerud A, Due-Tønnessen P, Fjell AM. 2009. Error-related negativity is mediated by fractional anisotropy in the posterior cingulate gyrus—a study combining diffusion tensor imaging and electrophysiology in healthy adults. Cereb Cortex. 19:293–304.
Westlye LT, Walhovd KB, Dale AM, Espeseth T, Reinvang I, Raz N, Agartz I, Greve DN, Fischl B, Fjell AM. 2009. Increased sensitivity to effects of normal aging and Alzheimer's disease on cortical thickness by adjustment for local variability in gray/white contrast: a multi-sample MRI study. Neuroimage. 47:1545–1557.
Wheeler-Kingshott CA, Cercignani M. 2009. About "axial" and "radial" diffusivities. Magn Reson Med. 61:1255–1260.
Woolrich MW, Jbabdi S, Patenaude B, Chappell M, Makni S, Behrens T, Beckmann C, Jenkinson M, Smith SM. 2009. Bayesian analysis of neuroimaging data in FSL. Neuroimage. 45:S173–S186.
Wozniak JR, Lim KO. 2006. Advances in white matter imaging: a review of in vivo magnetic resonance methodologies and their applicability to the study of development and aging. Neurosci Biobehav Rev. 30:762–774.
Yakovlev P, Lecours A. 1967. The myelogenetic cycles of regional maturation of the brain. In: Minkowski A, editor. Regional development of the brain in early life.. Oxford: Blackwell. p. 3–70.
Zahr NM, Rohlfing T, Pfefferbaum A, Sullivan EV. 2009. Problem solving, working memory, and motor correlates of association and commissural fiber bundles in normal aging: a quantitative fiber tracking study. Neuroimage. 44:1050–1062.